Cell Calcium 34 (2003) 499–509

cell calcium

www.elsevier.com/locate/ceca

Optical single-channel recording: imaging Ca^{2+} flux through individual N-type voltage-gated channels expressed in *Xenopus* oocytes

Angelo Demuro, Ian Parker*

Department of Neurobiology and Behavior, University of California, Irvine, CA 92697-4550, USA

Received 20 May 2003; received in revised form 23 June 2003; accepted 23 June 2003

Abstract

Functional studies of single membrane ion channels were made possible by the introduction of the patch-clamp technique, which allows single-channel currents to be measured with unprecedented resolution. Nevertheless, patch clamping has some limitations: including the need for physical access of the patch pipette, possible disruption of local cellular architecture, inability to monitor multiple channels, and lack of spatial information. Here, we demonstrate the use of confocal fluorescence microscopy as a non-invasive technique to optically monitor the gating of individual Ca^{2+} channels. Near-membrane fluorescence signals track the gating of N-type Ca^{2+} channels with a kinetic resolution of about 10 ms, provide a simultaneous and independent readout from several channels, and allow their locations to be mapped with sub-micrometer spatial resolution. Optical single-channel recording should be applicable to diverse voltage- and ligand-gated Ca^{2+}-permeable channels, and has the potential for high-throughput functional analysis of single channels.
© 2003 Elsevier Ltd. All rights reserved.

Keywords: *Xenopus* oocyte; Single-channel recording; N-type Ca^{2+} channel; Confocal microscopy

1. Introduction

The introduction of the patch-clamp technique by Neher and Sakmann [1,2] revolutionized our understanding of ion channel functioning by allowing measurement of single-channel currents with exquisite resolution. Nevertheless, the patch-clamp technique suffers some limitations. The channel of interest must be physically accessible to the patch pipette; seal formation may disrupt the local cytoskeletal architecture [3]; independent measurements cannot be obtained from multiple channels; and little information is provided regarding the spatial distribution of channels. Recent developments in optical techniques hold promise as an alternative, less invasive approach for monitoring the kinetic activity of multiple single channels. In particular, the use of highly sensitive fluorescent Ca^{2+} indicators [4] has permitted imaging of Ca^{2+} flux through clusters containing a few Ca^{2+}-permeable channels [5–7], and even through individual channels [8–12]. However, this approach had not previously provided sufficient resolution to study channel kinetics, and single-channel imaging has been restricted to channels with unusually high Ca^{2+} permeability and long open times [10,11], or to channels whose lifetime was pharmacologically prolonged [12]. Here, we employed high-resolution confocal microscopy to image Ca^{2+} flux through individual voltage-gated Ca^{2+} channels under physiological conditions, and demonstrate the utility of this methodology as a practicable, non-invasive tool to measure the functional kinetics and spatial localization of Ca^{2+}-permeable channels.

2. Materials and methods

2.1. Oocyte preparation and electrophysiology

Experiments were performed on defolliculated stage V and VI oocytes obtained from *Xenopus laevis* [13]. Plasmids containing cDNA clones coding for the N-type Ca^{2+} channel $\alpha_{1B\text{-}d}$ and β_3 subunits were linearized and transcribed in vitro [14], and equal quantities of each subunit cRNA were mixed to a final concentration of 0.1–1 μg/μl and injected (50 nl) into oocytes 3–5 days prior to imaging or electrophysiological recordings. Patch-clamp recordings were obtained in cell-attached mode, using a Gene Clamp 500 amplifier and the WCP (Strathclyde Electrophysiology

Abbreviations: IP_3, inositol 1,4,5-trisphosphate; ACh, acetylcholine; FWHM, full-width at half-maximal amplitude; CICR, Ca^{2+}-induced Ca^{2+} release

* Corresponding author. Tel.: +1-949-824-7833; fax: +1-949-824-2447.
E-mail address: iparker@uci.edu (I. Parker).

0143-4160/$ – see front matter © 2003 Elsevier Ltd. All rights reserved.
doi:10.1016/S0143-4160(03)00154-4

software) data acquisition package. Currents were filtered at 500 Hz (4-pole Bessel) and sampled at 1 ms. The patch pipette solution contained 110 mM $BaCl_2$, 5 mM HEPES, pH 7.5. The oocyte resting membrane potential was separately monitored by an intracellular microelectrode, and the patch potential was held at −60 mV and stepped to −20 or +20 mV during 1 s pulses delivered at 1 s intervals. Leak and capacitative currents were removed by subtracting averaged records without activity. Records of whole-cell Ba^{2+} currents were obtained using a two-electrode voltage-clamp, with oocytes bathed in a solution containing (in mM) NaCl, 110; $BaCl_2$, 5; KCl, 2; HEPES, 5; at pH 7.2. Records of Ca^{2+}-activated Cl^- currents were obtained in response to depolarization to +30 mV, in Ringer's solution containing 6 mM $CaCl_2$.

2.2. Ca^{2+} imaging

Oocytes were injected with fluo-4-dextran (MW 10,000 D) or Oregon Green 488 BAPTA-1 (OG-1) to a final intracellular concentration of about 40 μM, and were imaged 1 h later using a custom-built linescan confocal scanner interfaced to an Olympus IX70 inverted microscope [15]. Fluorescence excitation was provided by the 488 nm line of an argon ion laser, with the laser spot focused by a 40× oil immersion objective (NA 1.35) and scanned along a 50 or 25 μm line at rates of 2–8 ms per line. Emitted fluorescence was detected at wavelengths >510 nm through a confocal pinhole, providing lateral and axial resolutions of about 0.3 and 0.5 μm, respectively. Linescan images were constructed and analyzed using routines written in the IDL programming language (Research Systems Inc., Boulder, CO). In all linescan images, distance along the scan line is depicted vertically, time runs left to right, and Ca^{2+}-dependent changes in fluorescence (ΔF) are expressed as a pseudo-ratio relative to the mean resting fluorescence (F_o) at each pixel before stimulation. Scans were obtained from flattened areas of the animal hemisphere of the oocyte, imaged through a cover glass forming the base of the recording chamber. The bathing solution contained (in mM) NaCl, 110; $CaCl_2$, 6, KCl, 2; HEPES, 5; at pH 7.2. The membrane potential was clamped at a holding potential of −60 mV using a two-electrode voltage-clamp (Gene Clamp 500, Axon Instruments, Foster City, CA), and stepped to more positive potentials to induce opening of N-type Ca^{2+} channels expressed in the plasma membrane. Ca^{2+} indicators were obtained from Molecular Probes Inc. (Eugene, OR); all other reagents were from Sigma.

3. Results

3.1. Imaging Ca^{2+} flux through N-type channels

We used the *Xenopus* oocyte as a model cell system to image Ca^{2+} flux through channels expressed by $\alpha_{1B\text{-}d}$ and β_3 subunits of an N-type voltage-gated Ca^{2+} channel [14]. Defolliculated oocytes were injected with Ca^{2+}-indicator dye (usually fluo-4 dextran; 40 μM) and were voltage-clamped while bathed in Ringer's solution containing 6 mM $CaCl_2$. Recordings of Ca^{2+}-activated Cl^- current (T_{out} current) [16] evoked by depolarizations to +30 mV were used to assay expression of N-type channels: oocytes used for imaging gave currents of 5–10 μA, whereas non-mRNA-injected oocytes showed <100 nA. Confocal linescan images were acquired along a 50 μm scan line focused on the cell membrane. Fig. 1 shows representative images recorded during depolarizations to increasingly positive potentials from a holding potential of −60 mV. Ca^{2+} signals were first evident with polarization to about −25 mV, and then increased progressively with depolarizations up to about +30 mV. In some oocytes the amplitude of the Ca^{2+} signals then declined and was almost completely suppressed at +80 mV, but other cells still showed strong responses even at +100 mV (not shown).

Several observations indicate that these fluorescence signals arose owing to Ca^{2+} entry through expressed N-type channels. (1) No signals were observed in control (non-mRNA-injected) oocytes ($n > 10$). (2) Responses became smaller when extracellular [Ca^{2+}] was lowered from 6 to 1.8 mM ($n = 5$). (3) Signals were abolished by 2 μM extracellular Ni^{2+} ($n = 3$), a selective blocker of voltage-gated Ca^{2+} channels. (4) The progressive increase in Ca^{2+} signals at potentials positive to about −25 mV mirrors the voltage-dependent activation of N-type channels [14], and their suppression at strongly positive voltages is consistent with a reduced electrochemical driving force for Ca^{2+} influx near the Ca^{2+} equilibrium potential.

Strong depolarizations evoked biphasic fluorescence responses, comprising an initial, rapidly decaying transient followed by a maintained, or slowly rising plateau (Fig. 1A and B). In contrast, only a maintained signal was apparent at voltages less than −10 mV (Fig. 1C). Based on observations of biphasic whole-cell (Fig. 4A) and single-channel (Fig. 4D) Ba^{2+} currents, it is likely that the two components reflect the voltage-dependent inactivation of N-type channels. That is to say, weak depolarizations induce a low probability of channel opening which declines only slightly with time, whereas the opening probability is high immediately after strong depolarization but then falls rapidly to a lower, but more sustained level [14]. Moreover, we interpret the slow secondary rise in fluorescence during strong depolarization (Fig. 1A) to arise because Ca^{2+} ions entering through non-inactivated channels accumulate in the cytosol from where they are cleared relatively slowly.

We can further exclude the possibility that Ca^{2+}-induced Ca^{2+} release (CICR) from intracellular stores contributed to the fluorescence signals. Inositol 1,4,5-trisphosphate (IP_3) receptors constitute the sole intracellular Ca^{2+} release channels in *Xenopus* oocytes [17], and display CICR only in the presence of elevated IP_3 levels: which was not the case here. Moreover, depolarization-activated Ca^{2+} signals remained unchanged after blocking IP_3 receptors with 10 mM caffeine

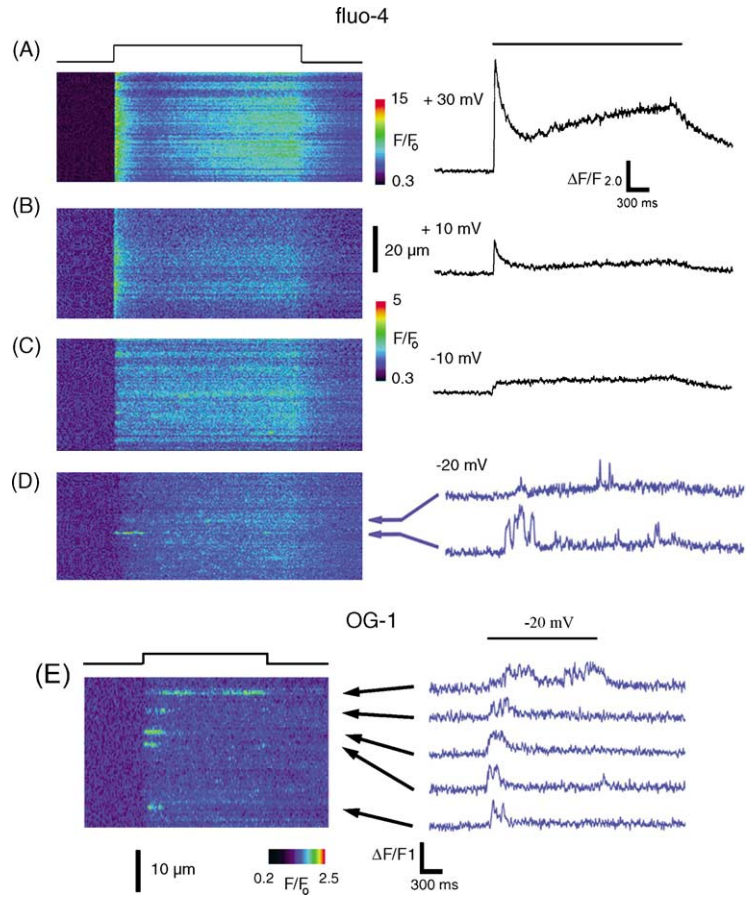

Fig. 1. Voltage-dependence of Ca^{2+} signals in oocytes expressing N-type Ca^{2+} channels. (A–D) Macroscopic and single-channel fluorescence signals in an oocyte loaded with fluo-4 dextran. Linescan confocal images show fluorescence Ca^{2+} signals evoked by depolarizing steps from −60 mV to the potentials indicated in millivolts. In each panel, distance along the scan line is depicted vertically, time runs left to right, and increasing fluo-4 fluorescence ratios (F/F_0: proportional to increasing $[Ca^{2+}]$) are represented as shown by the color bars. Note that the pseudocolor scale is different for the upper panel to encompass the wide dynamic range of the responses. Bar indicates the duration of the voltage steps. Black traces at the *right* show corresponding mean fluorescence measurements over 30 pixels (4 μm) regions as indicated. The blue traces show measurements of local (3 pixels average) fluorescence from the regions in (D) marked by the arrows that displayed sparklets. Records are representative of results in >15 oocytes. (E) Similar linescan image and fluorescent traces obtained from a oocyte loaded with Oregon Green-1, in response to depolarization from −60 to −20 mV.

[17], even though Ca^{2+} waves evoked in the same cells ($n = 3$) by photoreleased IP_3 were abolished.

Fluorescence signals evoked by strong depolarizations usually appeared spatially homogeneous (Fig. 1A), probably because numerous Ca^{2+} channels opened simultaneously and the resulting flood of Ca^{2+} influx precluded resolution of signals arising from individual channels. However, at more negative voltages the linescan images became increasingly 'streaky', and localized, stepwise transients were evident (Fig. 1D). On the basis of evidence presented below, we interpret these pulsatile signals to arise from Ca^{2+} flux through single channels and, following the nomenclature of Wang et al. [12], refer to them as 'sparklets'. The enhanced ability to resolve single-channel signals with weak depolarizations probably arose because only a few channels opened so that their Ca^{2+} flux could be better discriminated on a low background of resting $[Ca^{2+}]$; and because the single-channel Ca^{2+} current would be greater at increasingly negative voltages away from the Ca^{2+} equilibrium potential.

3.2. Indicator dyes

Most experiments were done using fluo-4 as the Ca^{2+} indicator, as the fluorescence of this probe is low in the absence of Ca^{2+}, but increases enormously (>15-fold) on binding Ca^{2+} [18]. Oocytes loaded with free fluo-4 showed strong compartmentalization of the dye after only a few minutes, but this problem was largely overcome by use of dextran-conjugated fluo-4. Moreover, the lower affinity (ca. 3 μM [18]) of the dextran conjugate would aid in localizing the fluorescence signal to regions of high $[Ca^{2+}]$ near the channel. Using fluo-4 dextran, sparklets showed peak fluorescence signals ($\Delta F/F$) as great as 5. We were also

able to image sparklets using Oregon Green-1 (Fig. 1E). This probe showed a higher resting fluorescence than did fluo-4, so that fluorescence ratio signals during sparklets were smaller (ca. $\Delta F/F = 1.7$). Nevertheless, the higher overall fluorescence of this dye provided brighter signals that, for a given laser power, had a signal-to-noise ration only slightly inferior to fluo-4.

3.3. Imaging single-channel Ca^{2+} transients

Fig. 2A illustrates sparklets arising autonomously at several localized sites in response to a weak (−20 mV) depolarization that gave a low probability of channel opening. As with the macroscopic fluorescence signals resulting from strong depolarizations, sparklets became smaller (but could still be resolved) when extracellular [Ca^{2+}] was lowered from 6 to 1.8 mM, and were not observed in control (non-mRNA-injected) oocytes. Successive events at a given site were of similar amplitude (except for filtering of brief events), but greater variability was seen between sites; presumably owing to differing proximity of channels to the scan line.

As with the macroscopic Ca^{2+} signals in Fig. 1, sparklets were little changed after applying caffeine (10 mM) to block IP_3 receptors, indicating that they arise solely through influx of extracellular Ca^{2+} across the plasma membrane without further 'amplification' by subsequent CICR from intracellular stores. Moreover, sparklets were tightly localized to the cell membrane such that their amplitude declined abruptly when the microscope was focused >2 μm into the cytosol. In contrast, IP_3 receptors are clustered more deeply in the endoplasmic reticulum and generate discrete Ca^{2+} release events ('puffs') that are maximal 4–10 μm inward from the surface membrane [13].

3.4. Channel-like artifacts

The voltage-dependent activation of pulsatile Ca^{2+} transients during depolarizing pulses in mRNA-injected oocytes provided strong evidence that these signals arose through Ca^{2+} influx through expressed N-type channels. We also observed two types of 'artifactual' fluorescence transients that mimicked the sparklets in some respects. However, these could be clearly distinguished, and records containing such artifacts were rejected before analysis. One signal appeared to result from Ca^{2+} influx through an unknown type of spontaneously active channel endogenously present in the oocyte membrane. These transients resembled sparklets in amplitude, durations, and spatial spread, but could be readily distinguished because they arose at negative (−60 to −120 mV) holding potentials, were seen in control as well as mRNA-injected oocytes, and reduced in amplitude during depolarizing pulses. A second artifact arose from bright, sub-resolution particles, akin to the 'streakers' previously described in skeletal muscle [19], which may arise through sequestration of indicator within small organelles having high [Ca^{2+}]. These particles were in constant motion, and produced transient streaks in linescan images as they crossed back and forth over the scan line. They were observed mostly in oocytes that had been loaded with fluo-4 >1 h before recording, and could be identified because of their shifting position along the scan line and occurrence regardless of membrane potential.

3.5. Kinetic analysis of sparklets

We next explored the utility of optical recording for analysis of channel kinetics by imaging several hundred sparklets during weak (−20 mV) polarizing pulses (Fig. 2B). No spontaneous events were observed at the holding potential (−60 mV) before or after depolarization, but local fluorescence signals occurred in an apparently stochastic manner throughout the voltage pulse. Their durations (measured at half-maximal amplitude) varied widely between <10 ms to several hundred milliseconds, and signals often arose as flickering bursts (e.g. second trace from top, Fig. 2Ba). The distribution of event durations (Fig. 2Bb) was well fitted by a single exponential, with a time constant of about 28 ms. There was, however, a fall-off in observations with durations <20 ms, likely reflecting missed brief events that were low-pass filtered by the optical recording. The latencies of sparklets during the depolarizing pulses followed double-exponential distributions (Fig. 2Bc), suggesting that the probability of channel opening was maximal immediately after depolarization and subsequently declined following two kinetic components.

To extend these studies to different voltages, we scanned the oocyte to find regions expressing a low density of channels (cf. Fig. 5C), where even strong depolarizations evoked only widely separated sparklets. The distribution of event durations at +20 mV (Fig. 2Ca and b) was similar to that at −20 mV, and fit a single exponential with a time constant of about 34 ms. However, the latencies of event occurrences during the pulse were markedly different between these two voltages. At +20 mV sparklets arose with high probability almost immediately following the onset of depolarization, and fewer events were observed during the remainder of the pulse (Fig. 2Ca). The distribution of event latencies thus showed two distinct components (Fig. 2Cc), with the relative amplitude of the first, rapidly decaying component being much greater than at −20 mV. This behavior mirrors the kinetics of the macroscopic Ca^{2+} signal shown in Fig. 1A and B, and presumably reflects voltage-dependent inactivation processes of the N-type Ca^{2+} channels.

Moreover, two patterns of inactivation were apparent during depolarization to +20 mV. Different to the characteristics illustrated in Fig. 2C, other channels showed no, or only a few sparklets following an initial event at the onset of depolarization (Fig. 2Ca), so that the second, slow component of the latency distribution was very small (Fig. 2Cc). This

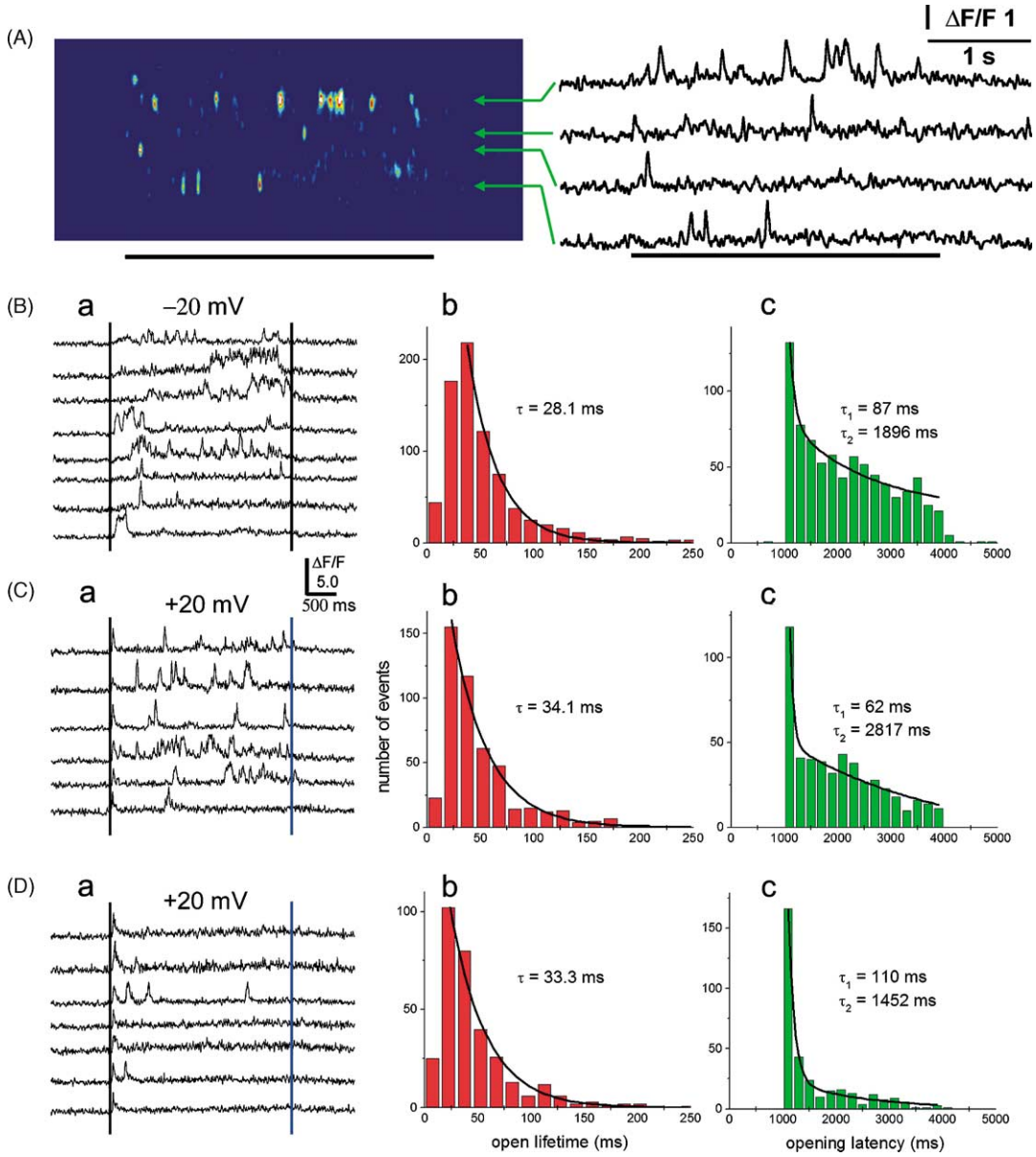

Fig. 2. Optical recording of Ca^{2+} flux through single voltage-gated channels. (A) Linescan image and corresponding fluorescence profiles illustrating single-channel events (sparklets). The oocyte expressed N-type voltage-gated channels and was depolarized from −60 to −20 mV as indicated by the bars. Fluorescence profiles were measured from 0.4 μm wide regions located as indicated by the arrows. (B) Kinetics of sparklets evoked by depolarization to −20 mV. (a) Traces show representative fluorescence measurements from eight different channels in response to voltage pulses from −60 to −20 mV, delivered between the blue lines. (b) Distribution of lifetimes of sparklets (duration at half-maximal amplitude: 794 events in seven oocytes). The black curve is a single-exponential fit, with time constant as indicated. (c) Corresponding measurements of latencies of all sparklets. The depolarizing pulse began at 1000 ms and ended at 4000 ms. The black curve is a double-exponential fit, with time constants as indicated. (C) Similar records and traces obtained during depolarizations to +20 mV. Data are from 500 channels (seven oocytes) that displayed multiple channel openings during the depolarizing pulse. (D) Data from other channels ($n = 334$: five oocytes) that displayed rapidly inactivating kinetics.

was not accompanied by any appreciable change in open durations (Fig. 2Cb).

3.6. Factors limiting kinetic resolution

Sparklet durations are, in principle, expected to follow a continuous exponential distribution, reflecting the underlying stochastic variation in open lifetimes of the Ca^{2+} channels. The fall-off in observations with durations <20 ms (e.g. Fig. 2Bb) is, therefore, likely to reflect a failure to resolve fluorescence signals arising from brief channel openings. Although fluorescent indicator dyes track large $[Ca^{2+}]$ elevations with sub-millisecond resolution [20], an ultimate limit to the temporal resolution of the optical recordings is set by the diffusion of Ca^{2+} and Ca^{2+}-bound indicator within the finite volume of the confocal spot. Our microscope

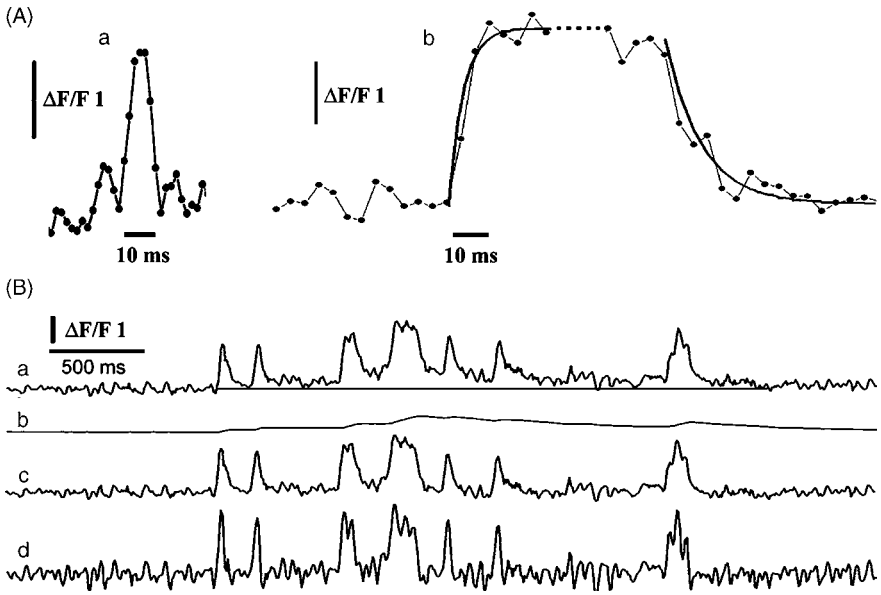

Fig. 3. Kinetic resolution of optical single-channel recording. (A) Trace in (a) shows a single, brief sparklet, recorded at a scan rate of 2 ms per line. Traces in (b) are averages of nine longer (>40 ms) sparklets, separately aligned to superimpose their rising and falling phases. Exponential curves fitted to the rising and falling phases have respective time constants of 4 and 10 ms. (B) Processing to improve the kinetic resolution of optical single-channel records. Traces show: (a) 'raw' fluorescence record displaying several sparklets at a single site; (b) estimated accumulation of intracellular Ca^{2+} resulting from the events in trace a, modeled as a 'leaky integrator' with a time constant of 600 ms; (c) fluorescence trace corrected for Ca^{2+} accumulation by subtracting trace b from trace a; (d) partial correction for low-pass filtering, obtained by summing trace c with its first derivative, using an empirically derived scaling factor with negative derivatives weighted 2.5-times greater than positive derivatives.

provides diffraction-limited optical performance (<0.1 fl confocal spot volume [15]), and is able to scan at rates as fast as 2 ms per line. In favorable cases, where we presume the laser scan fell directly on a channel, we could resolve 'square' events with durations <10 ms, and rise and fall times of ~4 ms (Fig. 3Aa). The filtering of events shorter than 20 ms in Fig. 2B–D is, therefore, sub-optimal, and likely resulted both from use of a slower (8 ms per line) scan rate in those experiments and inclusion of non-focal events.

Although brief events showed roughly symmetrical rise and fall times, the decay of fluorescence at the end of longer sparklets was slower than the rise (respective time constants about 4 and 10 ms: Fig. 3Ab), probably because the greater accumulation of Ca^{2+} around the channel was slower to dissipate. This latter factor also introduced a further distortion in the record, in that the basal fluorescence showed a slow rise throughout several hundred milliseconds during bursts of sparklets (Fig. 3Ba).

These limitations could be partially corrected by empirical post-processing of fluorescence measurements (Fig. 3B). First, the accumulation of Ca^{2+} during successive sparklets was simulated by treating the cytosol as a leaky integrator with a time constant of 600 ms. Subtraction of the resulting trace (Fig. 3Bb) from the 'raw' fluorescence record then yielded a baseline-corrected signal (Fig. 3Bc). Finally, this was processed using a high-frequency boost function, with asymmetrical weighting for positive- and negative-going signals, to compensate for the low-pass filtering of the optical system (Fig. 3Bd).

3.7. Optical versus electrophysiological recording

The introduction of a new optical approach to monitor channel function requires that it be validated against well-established electrophysiological measures. Our experimental system (inverted microscopy of large, opaque oocyte cells) did not allow us to obtain simultaneous patch-clamp and optical records from a given channel as achieved by others [10–12]. Instead, we obtained parallel whole-cell and single-channel currents from other oocytes expressing N-type Ca^{2+} channels, utilizing Ba^{2+} as the charge carrier [14] both to enhance the single-channel current and to minimize activation of Ca^{2+}-dependent Cl^- channels.

Fig. 4A shows whole-cell inward Ba^{2+} currents in response to voltage-clamp depolarizations to +20 and −20 mV. These may be compared with traces of mean Ca^{2+} flux, derived from optical single-channel records (Fig. 4B) by averaging baseline-corrected sparklet records like those in Fig. 2Ba and Ca. There is a close correspondence between the electrophysiological and optical measures. In both cases a marked inactivation of divalent cation influx is apparent at +20 mV, whereas influx declines only slightly at −20 mV.

A more detailed comparison was obtained from patch-clamp recording of single N-type channels in cell-attached patches (Fig. 4C). Using 110 mM Ba^{2+} as the charge carrier, the single-channel current was ~0.5 pA at −20 mV. We were unable to resolve individual openings (noise threshold ~0.2 pA) with 6 mM Ca^{2+} as used for fluorescence imaging. Measurements of mean channel open

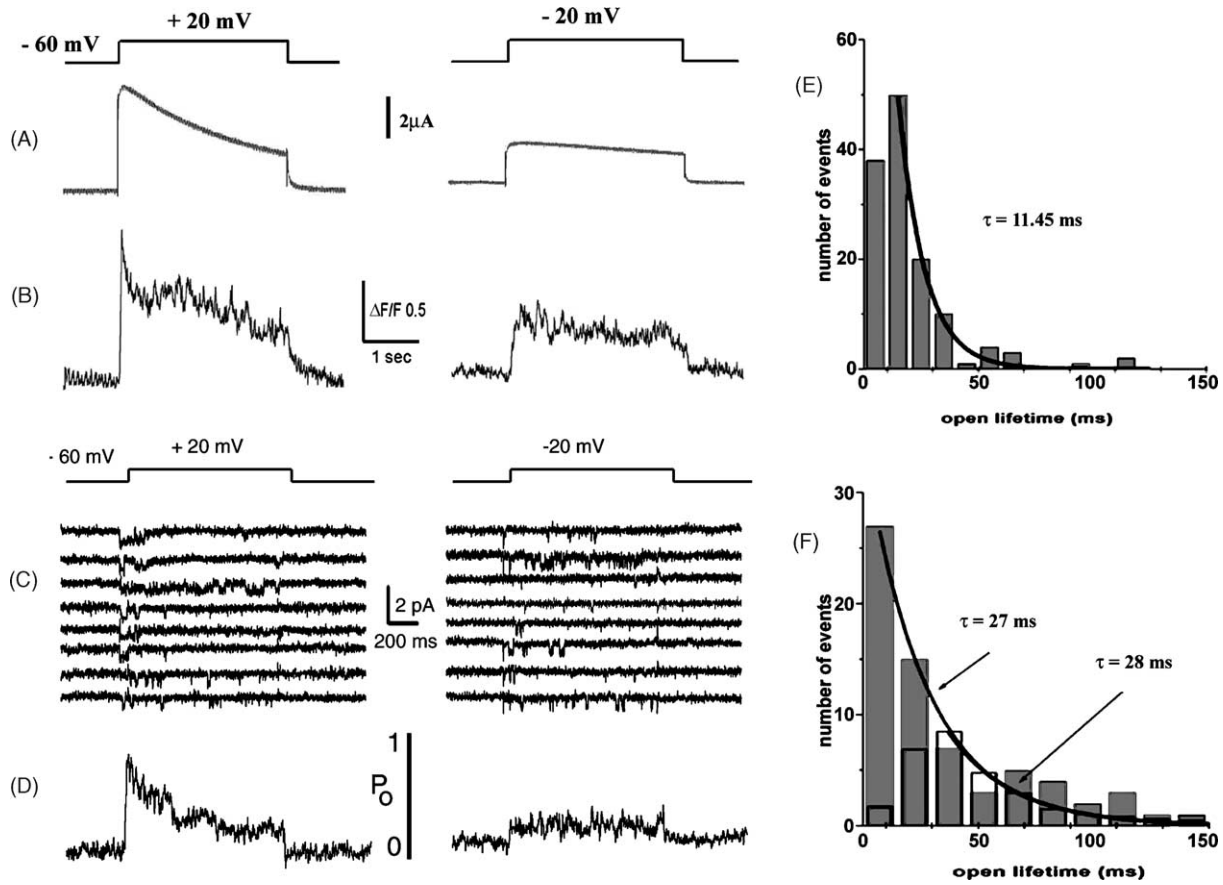

Fig. 4. Comparison of channel kinetics obtained by optical and electrophysiological recordings. (A) Whole-cell Ba^{2+} currents, recorded in an oocyte expressing N-type Ca^{2+} channels in response to depolarization from −60 to +20 mV (*left*) and −20 mV (*right*). (B) Measurements of kinetics of mean Ca^{2+} influx during depolarizing pulses, obtained from optical records like those in Fig. 2B and C by averaging traces of sparklet occurrence. (C) Patch-clamp recordings of N-type Ca^{2+} channels expressed in *Xenopus* oocytes. The pipette contained 110 mM Ba^{2+}, and the patch potential was stepped from −60 to +20 mV (*left*) and −20 mV (*right*). Single-channel openings (downward deflections, corresponding to inward membrane currents) were activated during polarization. (D) Mean channel open probability (P_o) as a function of time during depolarizing pulses, derived by averaging traces ($n = 37$) like those in panel C. (E) Distribution of channel open times obtained from patch-clamp data at −20 mV, recorded with 500 Hz bandwidth. Data are fitted by a single exponential, with time constant of 11.45 ms. (F) Re-analysis of the same patch-clamp recordings after excluding closings shorter than 20 ms, so as to simulate the low-pass filtering of optical recordings. The exponential curve has a time constant of 28 ms.

probability (P_o), derived by summing single-channel traces, showed kinetics that were again similar to optical measurements. That is to say, prominent inactivation was apparent at +20 mV, whereas P_o was more sustained, but smaller at −20 mV (Fig. 4D).

A discrepancy was, however, apparent in measurements of channel open durations. Patch-clamp records showed an excess of brief openings as compared to fluorescence recordings, and the distribution of open times followed a single exponential with a mean of 11.5 ms at −20 mV (Fig. 4E) versus 28 ms derived from unprocessed sparklets (Fig. 2Bb). Failure to resolve brief openings in the optical records would not account for this difference, because fitting to the sparklet data excluded events <25 ms. Instead, the discrepancy probably arose because the lower bandwidth of the optical recordings attenuated brief closings during bursts of openings, so that measurements of sparklet durations reflected that of the bursts, rather than their constituent openings. In agreement, re-analysis of the patch-clamp data excluding closings <20 ms yielded an exponential distribution of apparent open times (open bars, Fig. 4F) with a time constant (27 ms) closely matching that derived from sparklets.

3.8. Spatial spread and signal mass of sparklets

The spatial spread of fluorescence (full-width at half-maximal amplitude: FWHM) during sparklets was tightly restricted (0.55 μm during brief events and 0.72 μm at the end of long openings: Fig. 5A), and little greater than the point-spread function of the microscope (~0.3 μm) [15], indicating that Ca^{2+} remains restricted to within a few hundred nanometers. This tight localization of fluorescence permitted independent resolution of signals from channels spaced as close as 800 nm (Fig. 5B).

An approximate measure of the amount of Ca^{2+} involved in an elementary Ca^{2+} signal can be obtained from its signal mass [19,21]; defined as the volume integral of $\Delta F/F$ and calculated as mass = peak $\Delta F/F \times 0.6 \times \text{FWHM}^3$,

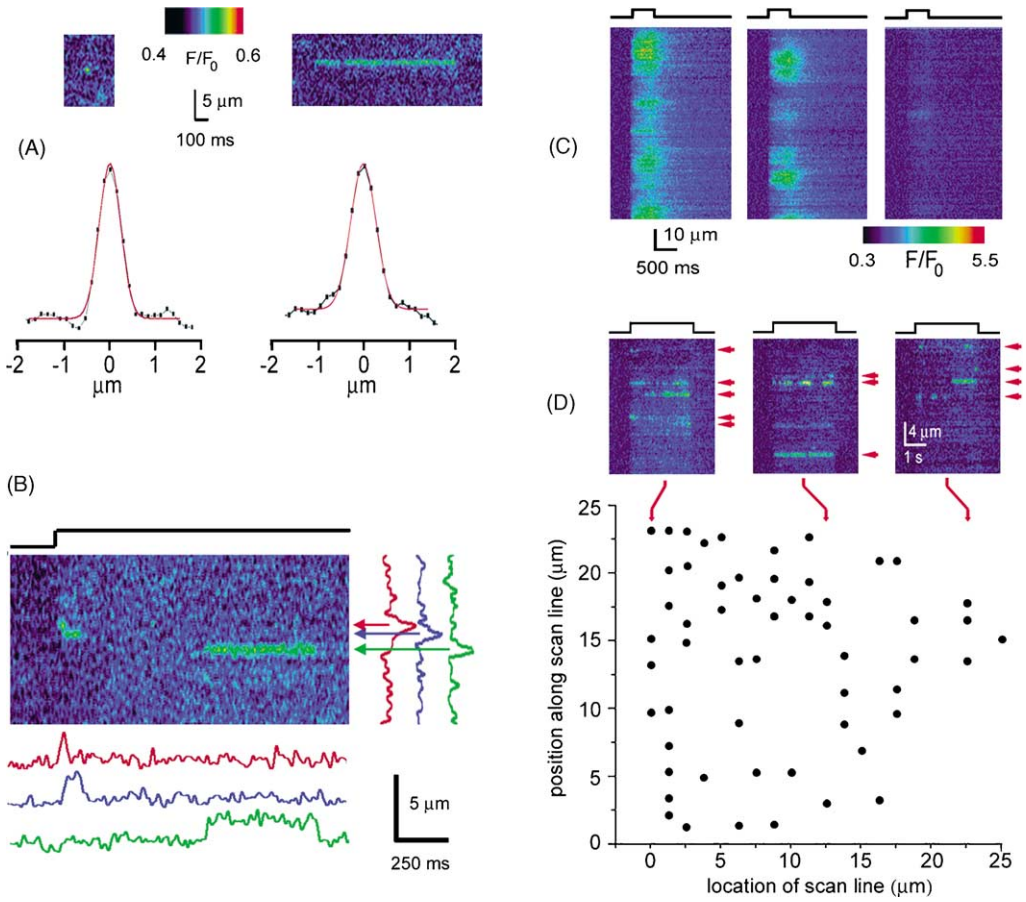

Fig. 5. Spatial aspects of sparklets. (A) Linescan images illustrate examples of brief and long sparklets. Plots show the spatial spread of fluorescence signal measured at the end of similar brief (*left*) and prolonged (*right*) sparklets. Data are normalized mean intensity profiles, averaged from six brief (≤10 ms) events and six long (>50 ms) events. Red curves are Gaussian fits, with respective widths (FWHM) of 0.56 and 0.72 μm. (B) Resolution of discrete channels separated by less than 1 μm. The linescan image shows events arising at three sites (colored arrows), evoked by polarization from −60 to −20 mV as indicated by the step. Traces show corresponding fluorescence measurements at these sites as functions of time (lower) and distance along the scan line (*right*). (C) Patchy variation in macroscopic density of channels in the oocyte membrane. The images show linescan Ca^{2+} signals recorded at three different locations about 200 μm apart in the same oocyte. The scans were focused at the plasma membrane, and the oocyte was stimulated by a 500 ms pulse from −60 to +20 mV. (D) Microscopic mapping of individual channels. Successive images (examples shown in the upper panels, with sparklets marked by arrows) were recorded at 30 s intervals as the laser line (25 μm long) was moved in increments of 1.25 μm along the *y* axis, so as to scan a 25 μm × 25 μm region of the membrane. At each *y* position, sparklets were evoked by a 3 s pulse to +20 mV, and their *x*–*y* coordinates were plotted to generate the map of channel locations shown in the lower panel.

assuming hemispherical distribution of Ca^{2+} from a point source in a planar membrane. For this purpose, we utilized linescan images obtained using Oregon Green-1 as the indicator, as we had previously calibrated signal mass with this dye in terms of moles of Ca^{2+} (a signal mass of 1 μm^3 is equivalent to roughly 2×10^{-20} mol Ca^{2+}, or a Ca^{2+} current of 4 pA for 1 ms) [21]. Measurements of brief (10–20 ms half-duration) sparklets imaged with Oregon Green-1 showed a mean signal mass of 0.17 ± 0.019 μm^3, corresponding to an underlying Ca^{2+} current of 0.037 ± 0.017 pA.

3.9. Mapping single Ca^{2+} channels

At a coarse scale, imaging of macroscopic Ca^{2+} signals evoked by strong depolarizations revealed a 'patchy' spatial distribution, with functional N-type Ca^{2+} channels concentrated within regions a few tens of micrometers across while neighboring regions of the membrane appeared almost devoid of channels (Fig. 5C). To demonstrate the capability for sub-micrometer mapping of individual channels, we selected a low density region, and applied strong depolarizations so that all channels would be likely to open at least once during each trial. The *x* coordinates of channels were located by identifying the positions of sparklets along the scan line, as marked by the arrowheads next to the linescan images in Fig. 5D. This procedure was then repeated as the scan line was stepped in increments of 1.25 μm along the *y* axis, so as to build up a two-dimensional map of channel locations within a 25 μm × 25 μm region of the oocyte membrane (lower panel, Fig. 5D). The mean density derived in this way was about 1 channel/10 μm^2; but this var-

ied considerably within the mapped region and was as high as 1 channel/3 μm^2 in some areas.

4. Discussion

The patch-clamp technique has been a mainstay of biophysical research on channel function for over 25 years. Nevertheless, patch-clamp recordings suffer some limitations. Our object in this paper is to demonstrate the potential of optical imaging as a practicable alternative, offering complementary advantages to electrophysiological measures of single-channel functioning.

We used the *Xenopus* oocyte as a model cell system to express voltage-gated N-type Ca^{2+} channels, and used high-resolution confocal microscopy to image localized, pulse-like fluorescence signals (sparklets) close to the cell membrane in response to membrane depolarizations. Several lines of evidence, presented above, indicate that the sparklets almost certainly arose as a result of Ca^{2+} influx through individual Ca^{2+} channels. In particular, sparklets were seen only in oocytes expressing N-type channels, they displayed unitary amplitudes and stochastic kinetics characteristic of single-channel behavior, they arose autonomously at discrete and well-separated sites, and their voltage-dependence and kinetics corresponded with electrophysiological measures of N-type channels. Moreover, it is unlikely that the sparklets reflected activity of clustered Ca^{2+} channels rather than individual channels. The magnitude of fluorescence signals was consistent with the expected single-channel current, and we did not observe double- or triple-size events as might be expected if multiple channels were active at a given locus.

4.1. Advantages of optical single-channel imaging

Optical imaging is inherently less invasive than patch-clamp recording, as there is no need for physical access of a patch pipette, and mechanical disturbance to the membrane and cytoskeleton associated with seal formation are avoided. Thus, it has the potential to monitor single-channel activity under physiological conditions from cells within intact tissues, and from organelles within a cell. Perhaps the greatest advantage arises, however, from the spatial information provided by imaging. Currents arising from multiple channels within a membrane patch are hard to disentangle and, although it is possible to achieve spatial mapping by successively patching a cellular region with multiple patch pipettes [22], this is exceptionally laborious and provides only a coarse localization. In contrast, the ability of imaging to provide independent readout from multiple channels and map their positions with sub-micrometer resolution is likely to facilitate studies of processes, such as channel clustering and diffusional mobility.

In principle, optical recording also provides an inherently greater amplification than does patch-clamp recording. A single Ca^{2+} ion passing through a channel contributes only two electron charges to the single-channel current, but an indicator molecule that binds Ca^{2+} can emit as many as 10^5 photons/ms with saturating excitation. In practice this sensitivity cannot be fully realized, as only a fraction of entering Ca^{2+} ions will bind to the indicator, and only a small fraction of the emitted photons are captured and detected by the confocal microscope. Nevertheless, we obtained good resolution of sparklets with near-physiological concentrations of extracellular Ca^{2+} (6 mM), whereas patch-clamp recordings almost invariably employ high concentrations of more permeant Ba^{2+} ions to enhance the single-channel current.

4.2. Limitations and prospects for improvements

The temporal resolution of channel openings in our experiments was at best about 10 ms. This is sufficient to provide useful information, but is an order of magnitude less than achieved by patch-clamp recording, and inadequate for a detailed kinetic characterization of channel gating. Although indicator dyes can track large (μM) Ca^{2+} transients with sub-millisecond resolution [20], a main limiting factor appears to be the diffusional spread of Ca^{2+} within the volume sampled by the confocal spot. Precipitous Ca^{2+} gradients (microdomains) exist around an open Ca^{2+} channel, such that concentrations >100 μM are likely at the channel mouth, but fall to <1 μM at distances of only about 1 μm [23,24]. Further, although $[Ca^{2+}]$ at the channel mouth almost instantly tracks the opening and closing of the channel, the concentration changes slow quadratically as a function of distance from the channel mouth. Attempts to speed the kinetic resolution, therefore, will hinge on more closely localizing the fluorescence signal. Incremental improvements may be possible by using lower affinity indicators to signal only the peak of the Ca^{2+} microdomain, and by applying algorithms to correct for local accumulation and dissipation of Ca^{2+} ions in the cytosol (cf. Fig. 3B). A fundamental limitation, however, is that the size of the confocal spot is set by the laws of optics, and cannot readily be reduced. Instead, different techniques that more closely localize measurements to the channel mouth hold greater potential—for example, the application of optical techniques, such as evanescent wave microscopy [25] or near-field recording [26], to provide an even thinner optical section, or by using Ca^{2+} indicators targeted to the cell membrane or specific channels.

The ability to record large fluorescent signals from the tiny amount of Ca^{2+} passing through a single-channel hinges on the availability of highly sensitive and selective Ca^{2+} indicators [4], coupled with the very low basal cytosolic $[Ca^{2+}]$ (ca. 50 nM) of resting cells. Recording of the flux of other ions (Na^+, K^+, Cl^-) through individual channels is, therefore, likely to be less practicable. Nonetheless, numerous voltage- and ligand-gated channels display appreciable Ca^{2+} permeability and should thus be amenable to this technique. For example, we have been able to record Ca^{2+}

signals from single muscle nicotinic acetylcholine channels (A.D. and I.P., unpublished).

4.3. Comparison with previous studies

Early confocal imaging studies [8,9] revealed fluorescence signals ('blips' and 'quarks') that were thought to arise from Ca^{2+} flux through single intracellular Ca^{2+} release channels: but in the absence of parallel electrophysiological measurements this interpretation could not be directly confirmed. An important breakthrough came with experiments where optical signals were observed synchronously with single-channel currents [10–12]. Zou et al. employed wide-field imaging of Ca^{2+} flux through caffeine-activated [10] and stretch-activated [11] channels in smooth muscle, in conjunction with whole-cell recording of channel currents. However, because of the large cytosolic volume from which fluorescence was measured, the wide-field optical signals had a slow time course and continued to rise throughout channel openings with durations as long as 100 ms. Different to this, Wang et al. [12] imaged Ca^{2+} flux through individual L-type channels in cardiac muscle, using confocal linescan microscopy similar to our imaging methodology. Their optical signals showed rise and fall times of about 20–30 ms, but involved use of both high (20 mM) extracellular [Ca^{2+}] and pharmacological prolongation of channel open time.

An alternative approach has used fluorescent reporters of protein structure to study function of single ion channels [27]. This method has important advantages in that it can provide information regarding conformational changes in channel structure, not merely channel opening, and is not restricted to Ca^{2+}-permeable channels. However, it suffers from weak signals and rapid photo-destruction, as only a one or a few fluorophores can be conjugated to each channel.

4.4. Applications for single-channel imaging

We envisage that optical single-channel recording will evolve as a powerful adjunct to the patch-clamp technique, as these methodologies have complementary advantages and limitations. Although optical recording does not inherently allow control of membrane potential or absolute measurement of single-channel current, it is less invasive, and permits spatially resolved, in situ monitoring of multiple channels, including those in locations inaccessible to a patch pipette. In addition to applications in basic research, optical single-channel recording holds promise for high-throughput screening of ion channel activity, based on a very different principle to current efforts aimed at developing massively parallel arrays of patch-clamp electrodes [28,29].

Acknowledgements

We thank Drs. Michael Cahalan and Peter Thorn for helpful comments and Diane Lipscomb for providing Ca^{2+} channel clones. Supported by NIH Grant GM-48071.

References

[1] E. Neher, B. Sakmann, Single-channel currents recorded from membrane of denervated frog muscle fibres, Nature 260 (1976) 799–802.
[2] O.P. Hamill, A. Marty, E. Neher, B. Sakmann, F.J. Sigworth, Improved patch-clamp techniques for high-resolution current recording from cells and cell-free membrane patches, Pflugers Arch. 391 (1981) 85–100.
[3] A.M. Gomez, B.G. Kerfant, G. Vassort, Microtubule disruption modulates Ca^{2+} signaling in rat cardiac myocytes, Circ. Res. 86 (2000) 30–36.
[4] A. Minta, J.P. Kao, R.Y. Tsien, Fluorescent indicators for cytosolic calcium based on rhodamine and fluorescein chromophores, J. Biol. Chem. 264 (1989) 8171–8178.
[5] I. Parker, Y. Yao, Regenerative release of calcium from functionally discrete subcellular stores by inositol trisphosphate, Proc. R. Soc. Lond. 246 (1991) 269–274.
[6] M.B. Cannell, H. Cheng, W.J. Lederer, The control of calcium release in heart muscle, Science 268 (1995) 1045–1049.
[7] H. Cheng, W.J. Lederer, M.B. Cannell, Calcium sparks: elementary events underlying excitation–contraction coupling in heart muscle, Science 262 (1993) 740–744.
[8] I. Parker, Y. Yao, Ca^{2+} transients associated with openings of inositol trisphosphate-gated channels in *Xenopus* oocytes, J. Physiol. 491 (1996) 663–668.
[9] P. Lipp, E. Niggli, Submicroscopic calcium signals as fundamental events of excitation–contraction coupling in guinea-pig cardiac myocytes, J. Physiol. 492 (1996) 31–38.
[10] H. Zou, L.M. Lifshitz, R.A. Tuft, K.E. Fogarty, J.J. Singer, Imaging Ca^{2+} entering the cytoplasm through a single opening of a plasma membrane cation channel, J. Gen. Physiol. 114 (1999) 575–588.
[11] H. Zou, L.M. Lifshitz, R.A. Tuft, K.E. Fogarty, J.J. Singer, Visualization of Ca^{2+} entry through single stretch-activated cation channels, Proc. Natl. Acad. Sci. U.S.A. 99 (2002) 6404–6409.
[12] S.Q. Wang, L.S. Song, E.G. Lakatta, H. Cheng, Ca^{2+} signalling between single L-type Ca^{2+} channels and ryanodine receptors in heart cells, Nature 410 (2001) 592–596.
[13] N. Callamaras, I. Parker, Radial localization of inositol 1,4,5-triphosphate-sensitive Ca^{2+} release sites in *Xenopus* oocytes resolved by axial confocal linescan imaging, J. Gen. Physiol. 113 (1999) 199–213.
[14] Z. Lin, S. Haus, J. Edgerton, D. Lipscombe, Identification of functionally distinct isoforms of the N-type Ca^{2+} channel in rat sympathetic ganglia and brain, Neuron 18 (1997) 153–166.
[15] I. Parker, N. Callamaras, W.G. Wier, A high-resolution, confocal laser-scanning microscope and flash photolysis system for physiological studies, Cell Calcium 21 (1997) 441–452.
[16] R. Miledi, I. Parker, Chloride current induced by injection of calcium into *Xenopus* oocytes, J. Physiol. 357 (1984) 173–183.
[17] I. Parker, I. Ivorra, Caffeine inhibits inositol trisphosphate-mediated liberation of intracellular calcium in *Xenopus* oocytes, J. Physiol. 433 (1991) 229–240.
[18] R.P. Haugland, Handbook of Fluorescent Probes and Research Products, 9th ed., Molecular Probes Inc., Eugene, OR.
[19] S. Hollingworth, J. Peet, W.K. Chandler, S.M. Baylor, Calcium sparks in intact skeletal muscle fibers of the frog, J. Gen. Physiol. 118 (2001) 653–678.
[20] M. Zhao, S. Hollingworth, S.M. Baylor, Properties of tri- and tetracarboxylate Ca^{2+} indicators in frog skeletal muscle fibers, Biophys. J. 70 (1996) 896–916.
[21] X.P. Sun, N. Callamaras, J.S. Marchant, I. Parker, A continuum of *Ins*P_3-mediated elementary Ca^{2+} signaling events in *Xenopus* oocytes, J. Physiol. Lond. 509 (1998) 67–80.
[22] D.O. Mak, J.K. Foskett, Single-channel kinetics, inactivation, and spatial distribution of inositol trisphosphate (IP_3) receptors in *Xenopus* oocyte nucleus, J. Gen. Physiol. 109 (1997) 571–587.

[23] M. Naraghi, E. Neher, Linearized buffered Ca^{2+} diffusion in microdomains and its implications for calculation of $[Ca^{2+}]$ at the mouth of a calcium channel, J. Neurosci. 17 (1997) 6961–6973.
[24] E. Rios, M.D. Stern, Calcium in close quarters: microdomain feedback in excitation–contraction coupling and other cell biological phenomena, Annu. Rev. Biophys. Biomol. Struct. 26 (1997) 47–82.
[25] D. Toomre, D.J. Manstein, Lighting up the cell surface with evanescent wave microscopy, Trends Cell Biol. 11 (2001) 298–303.
[26] F. de Lange, A. Cambi, R. Huijbens, B. de Bakker, W. Rensen, M. Garcia-Parajo, N. van Hulst, C.G. Figdor, Cell biology beyond the diffraction limit: near-field scanning optical microscopy, J. Cell Sci. 114 (2001) 4153–4160.
[27] A. Sonnleitner, L.M. Mannuzzu, S. Terakawa, E.Y. Isacoff, Structural rearrangements in single ion channels detected optically in living cells, Proc. Natl. Acad. Sci. U.S.A. 99 (2002) 12759–12764.
[28] F.J. Sigworth, K.G. Klemic, Patch clamp on a chip, Biophys. J. 82 (2002) 2831–2832.
[29] J. Xu, X.B. Wang, B. Ensign, M. Li, L. Wu, A. Guia, J. Xu, Ion-channel assay technologies: quo vadis? Drug Discov. Today 6 (2001) 1278–1287.